

# High-dimensional structure underlying individual differences in naturalistic visual experience

Chihye Han<sup>1</sup>, Michael F. Bonner<sup>1\*</sup>

<sup>1</sup>Department of Cognitive Science, Johns Hopkins University, Baltimore, MD 21218

\*Corresponding author. Email: mfbonner@jhu.edu

**How do different brains create unique visual experiences from identical sensory input? While neural representations vary across individuals, the fundamental architecture underlying these differences remains poorly understood. Here, we reveal that individual visual experience emerges from a high-dimensional neural geometry across the visual cortical hierarchy. Using spectral decomposition of fMRI responses during naturalistic movie viewing, we find that idiosyncratic neural patterns persist across multiple orders of magnitude of latent dimensions. Remarkably, each dimensional range encodes qualitatively distinct aspects of individual processing, and this multidimensional neural geometry predicts subsequent behavioral differences in memory recall. These fine-grained patterns of inter-individual variability cannot be reduced to those detected by conventional intersubject correlation measures. Our findings demonstrate that subjective visual experience arises from information integrated across an expansive multidimensional manifold. This geometric framework offers a powerful new lens for understanding how diverse brains construct unique perceptual worlds from shared experiences.**

# 1 Introduction

The human brain transforms visual input into subjective perceptual experiences. When presented with identical visual stimuli, individuals exhibit idiosyncratic patterns of neural activity across cortical regions involved in visual processing (1). Idiosyncratic neural activity patterns remain stable across time (2, 3) and carry meaningful information about behavior (2, 4). Individuals with shared personality traits (5), shared context (6), or shared perspectives (7) have more similar neural responses during naturalistic narrative experience. These findings underscore the importance of understanding differences in neural representations underlying differences in perception and behavior across people. However, the full extent of variability within rich neural structure that gives rise to unique visual experience remains largely unknown.

Here, we investigated the dimensionality of neural representational structure underlying individual differences. Specifically, we quantified the extent to which inter-individual variability can be characterized through latent codes spanning multiple dimensional ranges. In neural population coding, dimensionality refers to the minimum number of axes needed to specify each response’s position in representational space (8). A prevailing view in cognitive neuroscience holds that cortical representations embed complex, high-dimensional stimuli into lower-dimensional latent subspaces to support generalization (9, 10). However, recent studies leveraging large-scale neural datasets show that natural stimulus representations in visual cortex span at least thousands of dimensions, with dimensionality scaling unboundedly up to the limit of the data (11, 12). This observation suggests that neural representations are more high-dimensional than previously appreciated. Crucially, dimensions beyond the leading, high-variance components encode stimulus information that may be relevant for perception but is not well-characterized by conventional analyses (12). These findings raise a critical question: Are there reliable individual differences across many latent dimensions of neural responses during naturalistic visual experience, or are they concentrated in a subset of dimensions that explain most of the variance in neural data? If neural representations are organized across multiple scales of variance, then individual differences in these representations might similarly span many latent dimensions. Alternatively, although stimulus-related variance is embedded in high-dimensional subspaces, it is possible that only a low-dimensional subspace might be relevant for individual differences in visual experience (13–15).

In this work, we use cross-decomposition to examine individual differences across the full spectrum of dimensions underlying cortical population codes. Our method combines spectral analysis with cross-validated functional alignment to characterize how neural representations vary between individuals at multiple representational scales. Using fMRI data of subjects viewing naturalistic movies, we quantify both the reliability and behavioral significance of intersubject variability in movie-evoked neural responses throughout the visual cortical hierarchy. Our findings reveal that reliable individual differences in visual processing manifest as distinct coactivation patterns distributed across multiple scales of neural representation, from dominant patterns explaining large amounts of variance to subtler patterns explaining increasingly smaller amounts. Crucially, we find that intersubject variability patterns are qualitatively distinct at each dimensional range and cannot be explained by conventional intersubject correlation (ISC) measures, revealing unique aspects of individual neural processing distributed across multiple levels of granularity. These multidimensional neural response patterns predict individual differences in movie recall, with neural-behavioral correlations distributed over a wide range of representational dimensions. These results highlight the multiscale structure of individual differences and establish a new spectral framework that advances our understanding of the high-dimensional neural architecture underlying subjective visual experience.

## 2 Results

### 2.1 High-dimensional structure in cortical responses to movies

One key to understanding neural population codes is characterizing how variance is distributed across latent dimensions of neural activity. Traditional approaches like principal component analysis (PCA) decompose neural responses into orthogonal dimensions sorted by variance. However, PCA captures both stimulus-driven and noise-related variance, potentially obscuring reliable stimulus-evoked patterns. Here, we employ cross-decomposition (12) to isolate reliable stimulus-related variance in neural activity. Our approach isolates stimulus-dependent activations through cross-validation: basis sets derived from training data are used to compute covariance spectra on held-out test data. Like hyperalignment (16), cross-decomposition performs the Procrustes transformation

to map a pair of neural response data into a set of orthogonal latent dimensions that maximize the covariance between the data sets. Importantly, our method provides a spectral characterization of shared variance, decomposing the shared signal into latent dimensions ordered by explained covariance.

We hypothesized that stimulus-related variance in movie-evoked neural responses would be distributed across multiple orders of magnitude of latent dimensions. While previous work used cross-decomposition to estimate the dimensionality of neural representations evoked by natural images (12), it has not been previously applied to dynamic, naturalistic movie responses. Here we applied cross-decomposition to a dataset of 43 subjects viewing four naturalistic movies in an fMRI scanner (17). The dataset was originally curated to study individual differences in neural event segmentation during movie viewing and contained movie stimuli with highly varied content. Thus, these movies provide an excellent stimulus set for testing the generalization of our findings using held-out stimuli that are qualitatively distinct from the training stimuli. Specifically, we used a one-movie-out cross-validation scheme, which provided a stringent test of reliability. For a pair of subjects, we extracted shared latent dimensions from a training set of movies, with one movie held out for testing (Fig. 1a, left). During the testing phase, the held-out movie responses from both subjects were projected onto shared latent dimensions, yielding a cross-covariance spectrum for the held-out data (Fig. 1a, right). We averaged the cross-covariance spectra across movie-folds and repeated this procedure for every subject pair.

We applied this procedure to neural responses from a series of anatomically defined regions of interest (ROIs) spanning a processing hierarchy from low-level vision to high-level semantics, which we expect to be strongly modulated by movie stimuli (Fig. 1b). These regions included early visual regions, ventral visual stream, lateral visual stream, and higher-level regions in the posterior parietal and cingulate cortex (See Methods). These ROIs allowed us to examine on how movie-evoked responses are represented across the cortical hierarchy, from early visual processing to multimodal regions associated with complex semantic integration.

Movie-evoked responses showed a characteristic power-law distribution of variance across latent dimensions in all examined regions, with cross-validated covariance spanning multiple orders of magnitude in each region (Fig. 1c). The smooth decay in covariance values across ranks showed that movie-evoked information is distributed across many dimensions. To verify that the covariance

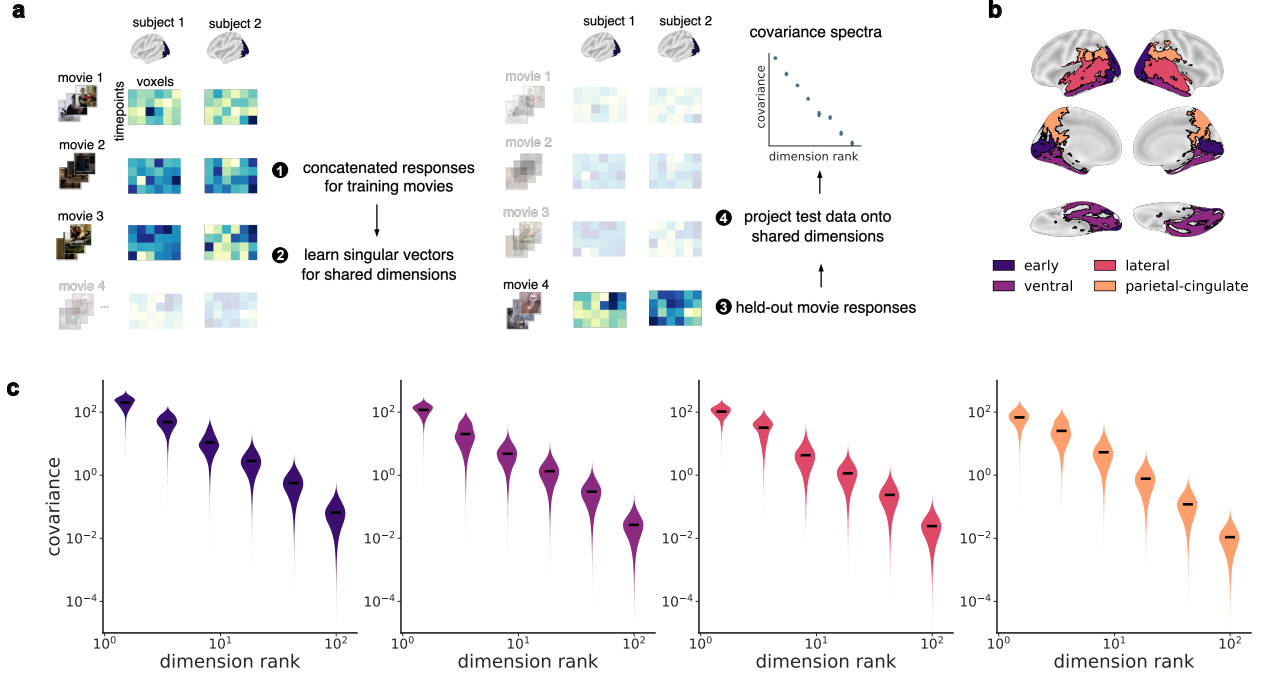


**Figure 1: Cross-decomposition analysis reveals many shared neural dimensions during movie viewing.** (a) One-movie-out cross-validated cross-decomposition is used to identify reliable neural signal. Left: Shared dimensions from a subject pair are extracted from neural responses to three movies, with one movie held-out for testing. Right: The held-out movie responses are mapped onto these shared dimensions ranked by the covariance on the training set, generating a covariance spectrum that quantifies the amount of reliable signal on the test data. The procedure is repeated for each held-out movie to yield an average spectrum for each subject pair. (b) Regions of interest (ROIs) spanning the cortical hierarchy from low-level vision to high-level semantics: early visual areas (purple), ventral temporal (violet), lateral temporal (red), and posterior parietal-cingulate (orange) regions. (c) Cross-validated covariance spectra for each ROI. Violin plots show the distribution of reliable covariance across all subject pairs. The reliable stimulus-related covariance follows a power-law distribution across dimension-rank in all regions, demonstrating that individual neural response patterns span multiple orders of magnitude rather than being confined to low-dimensional subspaces.

estimates over a wide range of ranks are statistically significant, we performed permutation tests by randomly block-shuffling movie-evoked responses across timepoints. We confirmed that up to 150 dimension ranks, the covariance statistics are significantly above the permuted spectra in all ROIs (Fig. S1). We thus focus on this range of dimensions for our analyses. We also examined the characteristic spatiotemporal scales of covariance patterns captured by each dimension and found a trend going from coarse- to fine-scale granularity across dimension ranks in both space and time (Fig. S2). Thus, the cross-decomposition analysis showed that the naturalistic movie viewing responses contained many dimensions of meaningful variance shared between individuals beyond the first few components, with successive dimensions reflecting finer patterns of cortical activity.

## 2.2 Individual differences in high-dimensional cortical response patterns

Having established that there is reliable variance spanning many dimensions, we next investigated whether these high-dimensional response patterns contain reliable information about individual variability. Although high-rank dimensions contain reliable stimulus-related signal, most variance in the data is concentrated in the first few dimensions. Thus, high-rank dimensions might not capture meaningful ways in which individuals differ in their neural processing. Alternatively, despite their decreased variance, higher-rank dimensions might nonetheless contain unique information about individual differences in neural processing that cannot be captured by the dominant lower-rank dimensions.

To investigate this, we characterized patterns of individual differences and assessed their reliability across different ranges of dimensions (Fig. 2a). We captured subject-by-subject similarity patterns of shared information in neural responses using individual differences matrices (IDMs) (18). We constructed IDMs for bins of latent dimensions for separate subsets of movies and computed the split-half reliability of individual differences across the full dimensional spectrum. If reliable individual differences span the full spectrum, this would indicate that the entire range of dimensions in these high-dimensional codes are potentially relevant to how individuals represent naturalistic stimuli. The reliability of individual differences in neural representations is important because it establishes the upper bound of the correlation between individual differences in neural codes and individual differences in behavior (19).

We found that individual differences were reliable across different subsets of movie stimuli throughout the entire spectrum of dimensions tested in all regions (Fig. 2b). The reliability of individual differences, quantified as correlations between IDMs derived from different sets of movies, remained significantly above zero at all dimensional ranges. This reliability was highest in low-rank dimensions but persisted even in high-rank dimensions, with statistically significant correlations extending to over a hundred dimensions in all examined regions (bootstrapped confidence intervals,  $n=1,000$  resamples;  $p < 0.05$ , Bonferroni-corrected).

These surprisingly stable individual differences in high-dimensional codes are brought out by the cross-decomposition procedure, which increases the detectability of stimulus-related signal and reveals fine-grained idiosyncrasies in neural responses. Specifically, functional alignment

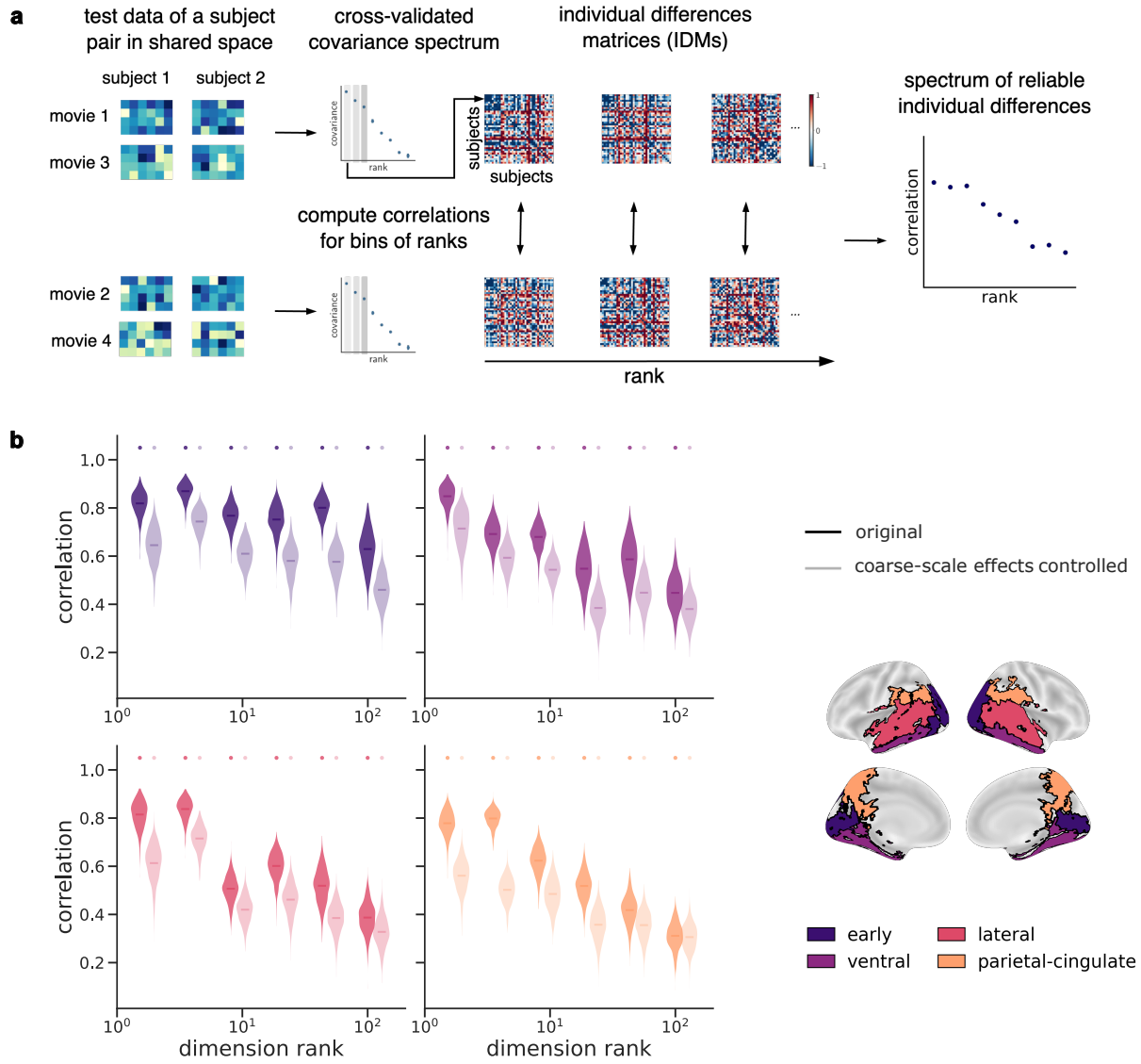


**Figure 2: Reliable individual differences persist across multiple dimensions of shared neural representations during movie viewing.** (a) Individual differences analysis compares patterns between independent sets of data to assess reliability. Covariance spectra are generated separately for neural responses to odd and even movies from each subject pair. These spectra are used to construct rank-wise individual differences matrices (IDMs), where red/blue colors indicate high/low dissimilarity between subjects (covariance values normalized for visualization purposes). Correlations between odd and even IDMs quantify reliability of individual difference patterns at each dimension rank, as shown in the hypothetical correlation plot on the right. (b) The observed correlations in all ROIs show significance across all examined dimension ranks up to two orders of magnitude. The persistence of significant correlations across high-dimensional ranks indicates that fine-grained neural response patterns in cross-validated covariance spectra contain reliable individual differences that cannot be reduced to simpler, coarse-scale properties detected by voxelwise intersubject correlation (ISC) measures. Violin plots show the bootstrap distribution of correlations between odd and even movie IDMs for each dimension rank bin, with 95% bootstrap confidence intervals ( $n=1,000$  resamples). Dark shades represent correlations between original IDMs; lighter shades show correlations after controlling for coarse-scale effects through partialing out voxelwise ISC IDMs. Dots above each violin indicate statistical significance ( $p < 0.05$ , Bonferroni-corrected).

transforms individual subjects' data into a shared representational space where fine-grained, multivariate patterns of activity captured in latent dimensions can be directly compared across subjects. To rule out the possibility that these high-dimensional effects can be explained by coarse response properties, we computed individual differences based on average voxelwise similarity and partialled out these similarity patterns from our IDMs at each dimensional range (see Methods). This control analysis isolates individual differences encoded in the multivariate pattern structure beyond what can be explained by coarse-grained voxel correlations.

While controlling for these coarse-scale effects modulated the magnitude of the IDM correlations, the overall pattern of reliable differences remained robust across the spectrum, and we continued to observe statistically significant reliability extending over a hundred dimensions in all regions (Fig. 2b). Thus, high-dimensional individual differences cannot be reduced to simpler, coarse-scale response properties but instead reflect differences in the fine-grained structure of neural representations.

After establishing that individual differences are reliable across many ranks, we next asked: do different dimensional ranges capture similar or distinct patterns of individual differences? If each range of dimensions reflects unique aspects of individual neural processing, we would expect the correlation between IDMs from the same dimensional range to be significantly stronger than correlations between different ranges. To test this hypothesis, we computed correlations between IDMs derived from different dimensional ranges across different sets of movies. The resulting correlation matrices revealed a prominent diagonal structure across all cortical regions. The strongest correlations were observed between matching dimensional ranges, with the mean correlation along the diagonal significantly higher than off-diagonal elements (Fig. 3a). This pattern was particularly pronounced after controlling for coarse-grained response properties (Fig. 3b), revealing fine-grained patterns of variability that were obscured by coarse-scale effects. Furthermore, region-to-region comparisons showed that removing the coarse-grained patterns of intersubject correlations also brings out ROI-specific patterns of variability at each dimensional range (Fig. S3). These results indicate that each range of latent dimensions not only contains reliable individual differences but captures qualitatively distinct patterns of individual neural processing. This dimensional specificity reveals that individuals meaningfully differ on multiple scales of naturalistic stimulus processing.



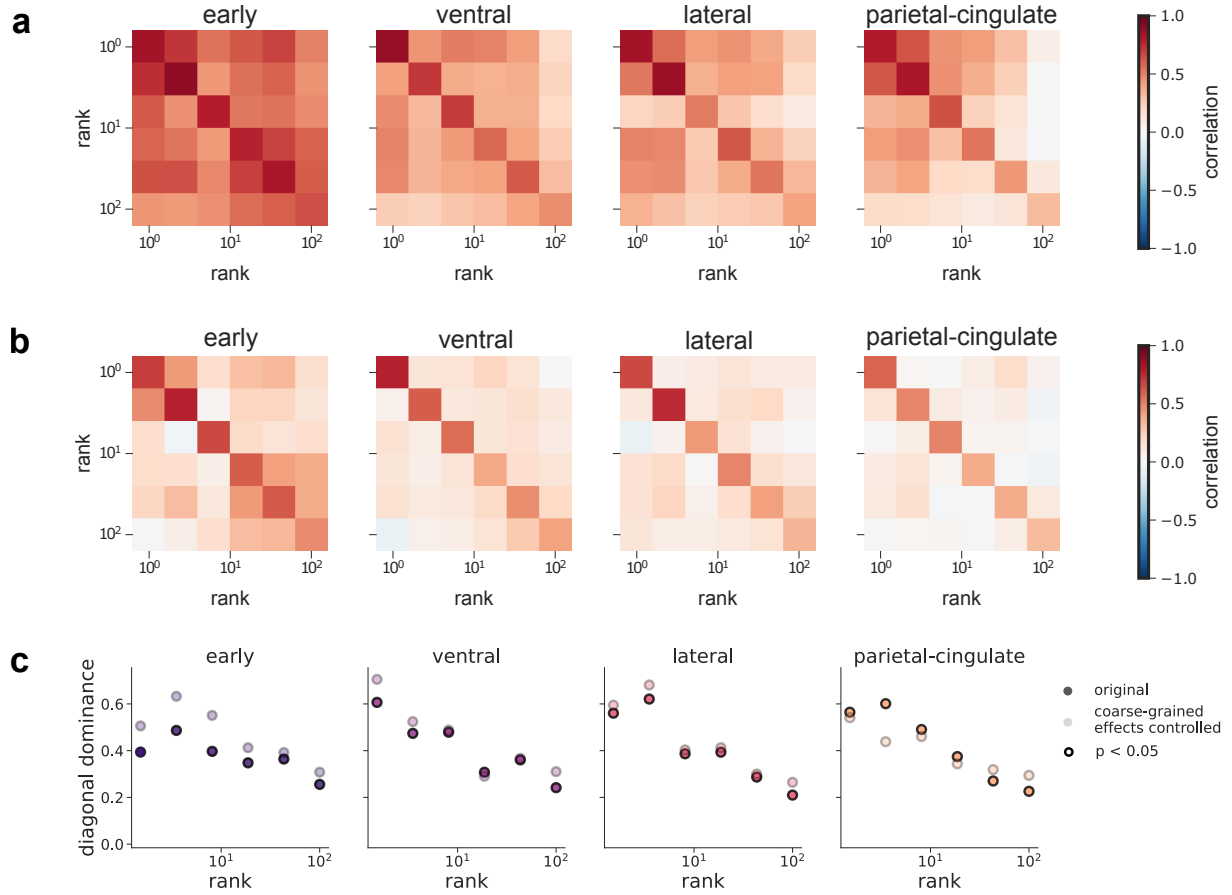


**Figure 3: Distinct patterns of individual differences emerge across different dimensional ranges.** (a) Correlation between individual difference matrices (IDMs) reveal stronger relationships between matching dimensional ranges than between different ranges. Each element represents the correlation between even-movie IDMs from one range (rows) and odd-movie IDMs from another range (columns). Diagonal values show same-range correlations that are consistently higher than off-diagonal values, indicating dimension-specific individual difference patterns. From left to right: early visual, ventral temporal, lateral visual, and posterior parietal-cingulate regions. (b) Same analysis after controlling for coarse-scale effects by partialing out voxelwise intersubject correlation (ISC) IDMs. The persistent diagonal structure indicates distinct, dimension-specific information in the residual, fine-grained patterns of individual differences. (c) Diagonal dominance (difference between on-diagonal correlation and mean off-diagonal correlation) remains significant across dimensional ranges before and after removing the coarse-grained effects. The diagonal dominance across ranks demonstrates that each dimensional range captures distinct aspects of individual neural processing during naturalistic viewing. Solid points show values from original matrices in **a**; lighter points show values after controlling for coarse-scale effects detected by conventional measures. All points shown are statistically significant (permutation tests,  $p < 0.05$ ).

## 2.3 Individual differences in cortical population codes and the interpretation of movies

Our analysis demonstrated that reliable individual differences span over a hundred dimensions in both low-level and high-level cortical regions. We next sought to understand whether these high-dimensional neural response patterns are behaviorally relevant to how individuals interpret movies. The dataset examined here is particularly well-suited for addressing this question because it includes behavioral data specifically designed to capture diverse interpretations of naturalistic stimuli.

To assess behavioral interpretations, we analyzed free recall transcripts collected after movie viewing. We used Google’s Universal Sentence Encoder (USE) to transform these transcripts into semantic embeddings that capture the conceptual content of each subject’s recall (Fig. 4a). For each movie, we constructed behavioral IDMs by computing pairwise correlations between subjects’ semantic embeddings, yielding a representation of the similarity structure in how individuals described and interpreted what they had seen. To test whether neural response patterns across different dimensional ranges predict behavioral similarities, we computed correlations between neural IDMs for each decade of latent dimensions and the behavioral IDMs.

We found that neural similarity patterns predict behavioral similarity across dimensional ranges spanning two orders of magnitude in all regions examined (Fig. 4b, left panel). These brain-behavior correlations remained significant up to dimensions in the 11-100 range across all cortical regions ( $p < 0.05$ , FDR-corrected). When controlling for coarse-scale effects, the correlation between neural and behavioral IDMs was attenuated across all regions but remained significant in the 11-100 dimensional range for the ventral, lateral, and posterior parietal-cingulate regions (Fig. 4b, right panel). In early visual cortex, the correlation between neural and behavioral IDMs was substantially reduced and no longer significant in the 11-100 range. Thus, while occipital regions contain coarse-grained information related to behavioral similarity, they lack fine-grained patterns that meaningfully correlate with individual differences in movie recall. In contrast, higher-level regions maintained behaviorally relevant information in fine-grained activity patterns after controlling for global response properties, suggesting that these subtle neural variations are important for capturing individual differences in stimulus interpretation.

The persistence of brain-behavior correlations across multiple dimensional ranges demonstrates

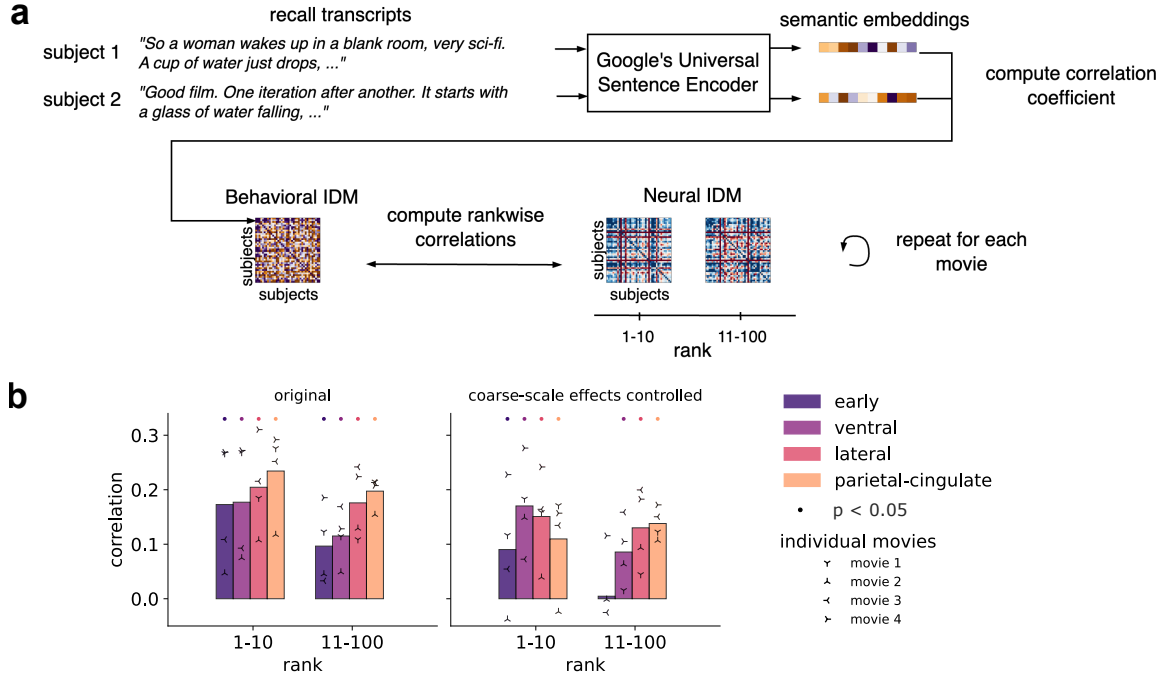


**Figure 4: High-dimensional neural patterns predict individual differences in subjective movie interpretations.** (a) Neural-behavioral correlation analysis links brain activity patterns to subjective experiences. Free recall transcripts from each subject are transformed into semantic embeddings using Google's Universal Sentence Encoder, generating subject-by-subject behavioral individual difference matrices (behavioral IDMs). These matrices capture similarities in how individuals interpreted and described the movies. Behavioral IDMs are then correlated with neural IDMs computed at different dimensional scales (1-10 and 11-100). Values of behavioral and neural IDMs are normalized for visualization purposes; Yellow/purple and red/blue colors indicate high/low dissimilarity between subjects in behavioral and neural IDMs, respectively. (b) Correlations between behavioral and neural patterns across cortical regions from early visual to posterior parietal-cingulate areas remain significant throughout multiple ranges of dimensions. Left panel shows raw correlations; right panel shows correlations after controlling for coarse-scale effects by partialing out voxel-wise inter-subject correlations. Higher-level regions (ventral, lateral, parietal-cingulate) maintain significant correlations at higher dimensional ranges even after controlling for coarse-scale effects. Dots above each bar indicate statistical significance ( $p < 0.05$ , FDR-corrected). Small triradiate symbols represent results for individual movies without averaging.

that behaviorally relevant individual differences extend well beyond the dominant dimensions that explain the majority of variance in neural responses. These findings reveal that each subject's unique perspective on naturalistic content is reflected in high-dimensional population codes distributed over a hundred dimensions in each region of the cortical hierarchy, suggesting that fine-grained neural response patterns typically overlooked in conventional analyses may be crucial for capturing the rich diversity of individual visual experiences.

### 3 Discussion

By applying cross-decomposition to fMRI data collected during movie viewing, we characterized the complex representational structure underlying individual differences. Strikingly, we found a remarkable persistence of reliable individual differences across this expansive dimensional spectrum. Our analyses revealed that even dimensions with relatively low variance contain stable information about individual neural processing. The dimensional specificity observed in patterns of individual differences provides compelling evidence for multiple orthogonal axes of variation in how individuals process identical visual stimuli. This dimensional specificity persisted even after controlling for coarse-scale response properties captured by voxelwise ISC measures, confirming that fine-grained multivariate patterns contribute substantially to neural individuality beyond what can be explained by coarse-grained responses. Lastly, the preservation of significant correlations between neural and behavioral similarity matrices across dimensional ranges further demonstrated that these high-rank dimensions, despite explaining relatively little overall variance, encode functionally meaningful information that shapes individual interpretations of visual input.

These findings bridge recent computational advances with fundamental questions about neural coding. Large-scale modeling efforts (20–25) and big-data approaches in neuroscience (26–28) have enabled empirical estimates of latent dimensionality that are orders of magnitudes greater than previously possible. Recent work in systems neuroscience found that cortical representations are high-dimensional (11, 12, 28–30), in line with theoretical perspectives suggesting that high-dimensional neural codes confer computational advantages for complex tasks (8, 30, 31). Our work extends this framework to the neural basis of individual differences and demonstrates that neural population codes leverage their full high-dimensional capacity to organize shared and idiosyncratic features across multiple representational ranges. Critically, our findings connecting high-dimensional neural patterns to individual differences in movie recall suggest that subjective experience emerges not from dominant neural signals alone, but from the integration of information distributed across the entire variance spectrum.

While previous work has shown that hyperalignment approaches improve detection of fine-grained individual differences by mapping responses to shared spaces (16, 18, 32, 33), these previous studies did not examine the range of latent dimensions that contribute to these individual differences.

Our spectral approach, which examines stimulus-related variance across the full spectrum of latent dimensions, reveals that individual differences manifest uniquely at each dimensional range—from dominant patterns in low-rank dimensions to subtle variations in high-rank dimensions. By explicitly modeling the distribution of variance across the full dimensional spectrum, our analysis reveals that high-rank dimensions encode qualitatively distinct and behaviorally significant information. Thus, our geometric perspective suggests focusing on the distribution and organization of variance across dimensions and provides a framework for characterizing the multiscale structure of neural individuality during naturalistic perception.

Several important questions remain. We demonstrated that different dimensional ranges capture distinct patterns of individual variability, but the specific representational content encoded within each range is left uncharacterized. Computational modeling approaches or targeted experimental manipulations could help interpret what cognitive features these dimensions represent—for instance, comparing neural patterns to representations from neural networks might reveal whether low-rank dimensions encode concrete, perceptual features and high-rank dimensions capture abstract, semantic information. Relatedly, it remains to be shown how high-dimensional representational structure transforms across the cortical hierarchy. We identified region-specific patterns of individual differences across dimensional ranges, but the evolution of these representations along the visual processing stream requires further investigation (34). Lastly, whether individual differences in variance distributions can be linked to trait-like phenotypes is an open question. Investigating the full dimensional structure of neural responses could identify subtle perturbations in how individuals with perceptual or cognitive disorders organize information across representational scales. For example, atypical sensory processing in neuropsychiatric conditions may manifest as altered distributions of information across neural dimensions, revealing neurobiological signatures undetectable through conventional measures of regional activation or connectivity (35–39). Future work should investigate these questions to develop a more complete understanding of how neural geometry shapes individual visual experience.

Together, our findings reveal that individual differences in visual processing manifest through high-dimensional neural codes distributed across multiple representational scales throughout the cortical hierarchy. This multiscale organization calls for approaches that capture the full spectrum of neural variability to comprehensively characterize the neural basis of individualized perceptual

experience. This geometric perspective reframes our understanding of neural individuality—not as variation along a few principal dimensions, but as a complex, high-dimensional pattern of idiosyncrasies distributed throughout representational space. Such a framework offers promising new avenues for investigating individual differences in perception, cognition, and potential alterations in clinical populations.

## Methods

### 3.1 Naturalistic fMRI dataset

We analyzed fMRI data from 42 subjects viewing four audiovisual movies (17). We excluded one subject whose recall data were missing from the original dataset (n=43). Movie durations ranged from 7:27 to 12:27 minutes and varied in content and cinematic style, including social and affective elements and screen cuts. Three out of four movies depicted scenarios with social interactions (versus one with purely mechanical actions), and two contained screen cuts (versus continuous camera panning).

**fMRI preprocessing** Functional images (TR=1 s) were preprocessed using fMRIPrep (40), including motion correction, co-registration, and normalization to MNI space at 2mm isotropic resolution. Preprocessed data were trimmed to movie segments and high-pass filtered (64 s cutoff) using FSL (41).

**Region of interest (ROI) definition** We defined four anatomical regions of interest (ROIs) spanning the visual cortical hierarchy using the Automatic Anatomical Labeling atlas (AAL3) (42): the early visual regions (including calcarine, superior, middle, and inferior occipital cortices), the ventral visual stream (including lingual, fusiform, inferior temporal, and parahippocampal cortices), and the lateral visual stream (including middle and superior temporal cortices). We also created an ROI by combining higher-level regions in the posterior part of the cortex (including supramarginal and angular gyri, precuneus, and posterior cingulate cortex) that we collectively refer to as posterior parietal-cingulate ("parietal-cingulate"). We grouped these high-level posterior regions to maintain comparable voxel counts across ROIs while combining regions that support similar semantic and multimodal integration functions. The covariance spectra patterns show similar high-dimensional structure when these posterior regions are analyzed separately. ROI masks were applied to each subject's preprocessed movie fMRI responses to extract the corresponding voxel timeseries matrices. All regions included both left and right hemispheres.

## 3.2 Cross-decomposition

**Estimating latent dimension** We used cross-decomposition to estimate the dimensionality of the latent neural subspace shared by pairs of individuals. For each subject pair, we analyzed their data matrices  $X, Y \in \mathbb{R}^{t \times v}$  representing  $t$  timepoints and  $v$  common voxels from subjects  $i$  and  $j$ , respectively. We computed the training set cross-covariance eigenvalues and eigenvectors using singular vector decomposition:

$$\text{cov}(X_{train}, Y_{train}) = U \Sigma V^T \quad (1)$$

The cross-covariance eigenspectrum for the testing set was then derived as:

$$\Sigma_{test}^{(i,j)} = \text{cov}(X_{test}U, Y_{test}V) \quad (2)$$

This procedure was applied using leave-one-movie-out cross-validation across all subject pairs. Spectra for all test movies and subject pairs were aggregated by computing the mean covariance within logarithmically-spaced bins of latent dimensions. For each bin, we calculated a representative center value  $c$  as the geometric mean of its edges and assigned each dimension rank to its corresponding bin. The binning approach allowed characterizing distributed aspects of neural representation.

**Permutation testing** Statistical significance was assessed through block permutation tests to maintain the temporal structure in fMRI data. We permuted 6-second blocks of movie timeseries and recomputed the cross-decomposition procedure to generate a null distribution.

**Spatial visualization** We visualized the spatial loadings of latent components on cortical surface models to examine how neural patterns change across dimension ranks. For each region, we extracted the left singular vectors ( $U$ ) of a sample pair from the cross-decomposition analysis, which represent the spatial loadings of each dimension. These loading patterns from individual dimensions were visualized with consistent thresholding (0.0001) and spatial smoothing (FWHM=2mm). Region-specific views were used to optimally display each ROI: medial views for posterior parietal-cingulate regions, ventral views for ventral temporal regions, and lateral views for early visual and lateral temporal regions.



**Temporal autocorrelation analysis** To quantify the temporal dynamics of different dimensional ranges, we computed autocorrelation functions for the time series associated with each latent dimension. First, we projected a sample subject’s fMRI data onto the shared latent dimensions derived from cross-decomposition. For each dimension, we computed the temporal autocorrelation function:

$$R(\tau) = \frac{1}{T - \tau} \sum_{t=1}^{T-\tau} (x_t - \bar{x})(x_{t+\tau} - \bar{x}) \quad (3)$$

where  $\tau$  represents the time lag in seconds,  $T$  is the total number of timepoints,  $x_t$  is the projected time series for a given dimension, and  $\bar{x}$  is the mean of the time series. Dimensions were grouped by rank (1-10, 11-50, 51-100, 101-200), and mean autocorrelation functions were calculated for each group. To quantify characteristic timescales, we fitted an exponential decay function to each dimension’s autocorrelation:

$$R_{fit}(\tau) = a \cdot e^{-\tau/\tau_0} \quad (4)$$

where  $\tau_0$  represents the characteristic decay time constant.

### 3.3 Reliable individual differences

To assess whether there is reliable individual *variability* along the ranks of these high-dimensional spectra, we constructed individual differences matrices (IDMs) that capture the pairwise similarities of subjects (18). For each logarithmic bin  $\kappa$  of latent dimensions, each cell of an IDM was computed from a pair of subjects  $i$  and  $j$  as:

$$IDM_c(i, j) = \Sigma_{test,c}^{(i,j)} \quad (5)$$

where  $\Sigma_{test,c}^{(i,j)}$  represents the cross-validated covariance for the bin centered at  $c$ . These IDMs reflect individual differences in representations across segments of latent dimensions. Covariance values in IDMs displayed in Fig. 2 and 3 were normalized to z-scores for visualization only and statistical analyses were performed on raw covariance values.

After regressing out head motion confounds (intersubject framewise-displacement correlations and median framewise-displacement similarities) from (17), we assessed reliability by computing Spearman correlations between mean IDMs derived from even and odd movies:

$$\rho_c = \rho(IDM_c^{even}, IDM_c^{odd}) \quad (6)$$

**Controlling for voxelwise structure** To distinguish fine-grained multivariate patterns from coarse-grained global effects, we constructed voxelwise inter-subject correlation (ISC) matrices. For each pair of subjects, we computed the mean Pearson correlation across all voxels in their response timeseries:

$$IDM_{ISC}(i, j) = \frac{1}{v} \sum_{k=1}^v r(X_{test,k}, Y_{test,k}) \quad (7)$$

where  $X_{test,k}$  and  $Y_{test,k}$  represent the response timeseries for voxel  $k$  in subjects  $i$  and  $j$ , respectively. We then assessed whether the fine-grained patterns captured by our dimensional approach contained information beyond these coarse-scale similarities by computing partial correlations:

$$\rho'_c = \rho(IDM_c^{even}, IDM_c^{odd} \mid IDM_{ISC}^{even}, IDM_{ISC}^{odd}) \quad (8)$$

where the partial correlation was computed by applying Spearman correlation to the residuals after regressing out the ISC matrices.

**Bootstrapped confidence intervals** To estimate confidence intervals, we implemented a bootstrap procedure with 1,000 resamples. For each resample, we randomly selected 90% of subjects with replacement and recomputed IDM correlations, excluding self-similarity values (43). This generated a correlation distribution for each rank bin, from which we derived 95% confidence intervals. We computed IDM correlations both before and after partialing out ISC effects, with FDR correction applied when comparing differences between these conditions.

**Dimensional specificity** To examine whether different ranges of latent dimensions capture distinct patterns of individual differences, we computed correlations between IDMs from different dimensional ranges. For each dimension bin  $c$ , we computed correlations between its even-movie IDM and odd-movie IDMs from all ranges. We then quantified the specificity of individual differences by comparing the diagonal elements (same-range correlations) to the mean of off-diagonal elements (different-range correlations) in each row. The diagonal dominance was computed by subtracting different-range correlations from the same-range correlations at each range.

To examine regional specificity of individual differences, we extended our IDM correlation approach across regions. We constructed a correlation matrix examining the relationships between IDMs from all combinations of dimensional ranges and cortical regions. Specifically, for each

region pair (early visual, ventral temporal, lateral temporal, and posterior parietal-cingulate) and each dimensional range pair, we computed Spearman correlations between even-movie IDMs from one region-range combination and odd-movie IDMs from another. We conducted this analysis both with original IDMs and after controlling for coarse-scale effects through the partial correlation procedure described above.

### **3.4 Neural-behavioral similarity analysis**

To examine relationships between neural individual differences and subjective movie interpretations, we analyzed the free recall data from (17). Following the original study, we used transcribed verbal descriptions collected after each movie viewing. These descriptions were encoded into a 512-dimensional semantic space using Google’s Universal Sentence Encoder (44). We constructed behavioral similarity matrices by computing pairwise cosine similarities between participants’ semantic embeddings.

We examined whether pairs of subjects with similar neural representational structure showed similar movie interpretations. First, we regressed out head motion confounds from all matrices. Then, we computed Spearman correlations between the behavioral similarity matrices and neural IDMs across two specific ranges of latent dimensions (1-10 and 11-100). This analysis was performed both with the original neural IDMs and with IDMs after controlling for voxelwise ISC matrices through partial correlation, allowing us to assess whether fine-grained neural patterns specifically contributed to behavioral similarities.

Statistical significance was assessed through permutation tests with 1,000 iterations. For each iteration, subject indices were randomly shuffled to generate a null distribution of neural-behavioral correlations. P-values were computed as the proportion of permuted correlations exceeding the observed correlation and were FDR-corrected across dimensional ranges.

### **3.5 Data availability**

The naturalistic audio-visual movie fMRI dataset is available at: <https://openneuro.org/datasets/ds004516>.

### **3.6 Code availability**

All code for analyses are available at: <https://github.com/kelseyhan-jhu/idiosyncratic-neural-geometry>.

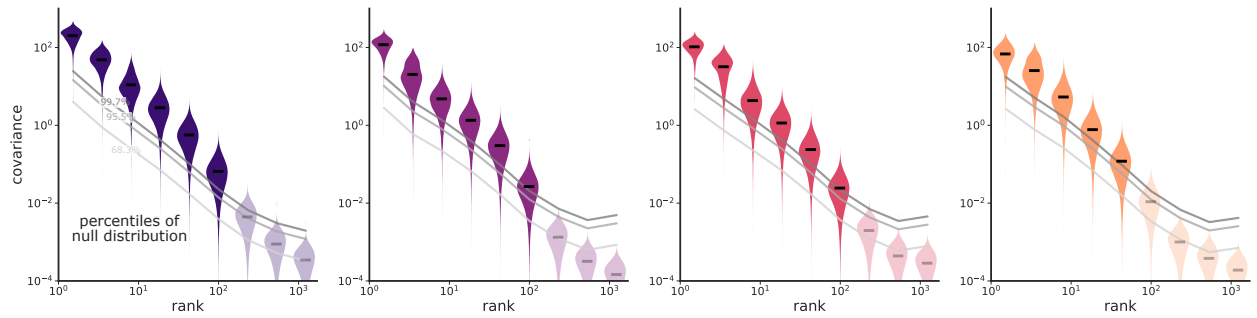


**Figure S1: Statistical validation of high-dimensional shared neural responses during movie viewing.** Permutation tests confirm reliable stimulus-related variance extends to over hundred dimensions. This analysis establishes the statistical reliability of the high-dimensional shared neural representations analyzed in the main text. Grey lines indicate statistical thresholds (99.7%, 95.5%, and 68.3% percentiles) of null distributions generated by randomly block-shuffling movie-evoked fMRI responses across timepoints. The null distributions also display scale-dependent decay because the analysis reports covariances—the distribution is centered at zero at each rank but reflects the scale of variance at that dimensional bin. Dark violin plots show the distribution of observed cross-validated covariance values, which remain significantly above the 99.9% percentile of the null distribution up to approximately 150 dimensions in all regions. The separation between observed data and null distributions confirms that stimulus-related information extends across many latent dimensions, beyond what would be expected by chance. From left to right: early visual, ventral temporal, lateral temporal, and posterior parietal-cingulate regions.

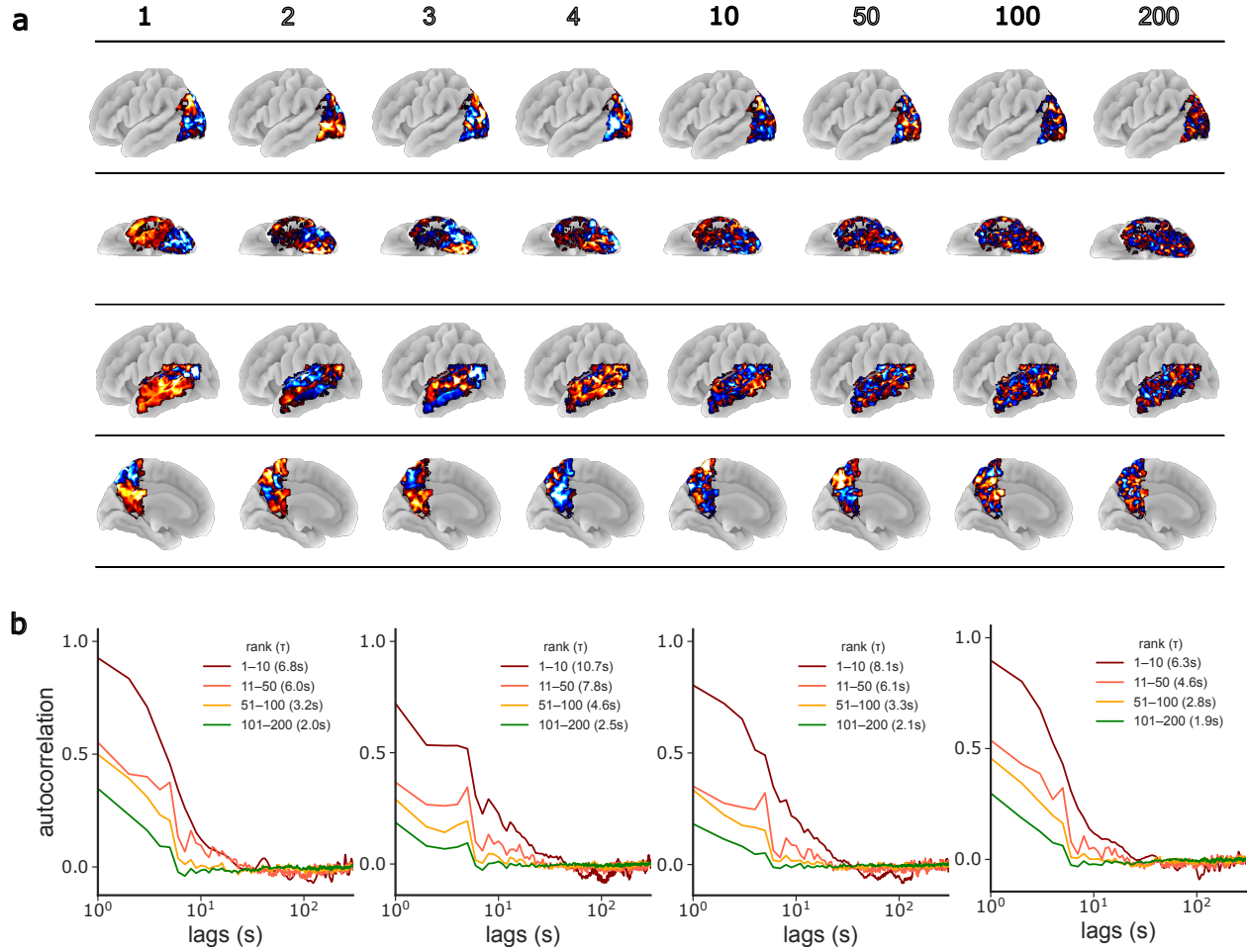


**Figure S2: Latent dimensions reveal systematic spatiotemporal organization from coarse to fine patterns.** (a) Visualization of latent component loadings across dimension ranks (numbers above each brain) demonstrates a hierarchical organization of neural activity patterns. Low-rank dimensions (1-10) capture large-scale spatial patterns with high variance, while higher-rank dimensions progressively represent finer-grained spatial structure. From top to bottom: early visual, ventral temporal, lateral temporal, and posterior parietal-cingulate regions. (b) Temporal autocorrelation analysis quantifies the timescale of neural dynamics across dimension ranks. Plots show autocorrelation values as a function of time lag (in seconds) for different dimensional ranges. From left to right: early visual, ventral temporal, lateral temporal, and posterior parietal-cingulate regions. Higher-rank dimensions (green lines) show faster temporal fluctuations with shorter autocorrelation timescales compared to lower-rank dimensions (red and brown lines), revealing a systematic relationship between spatial and temporal scales across the dimensional hierarchy within each cortical region.

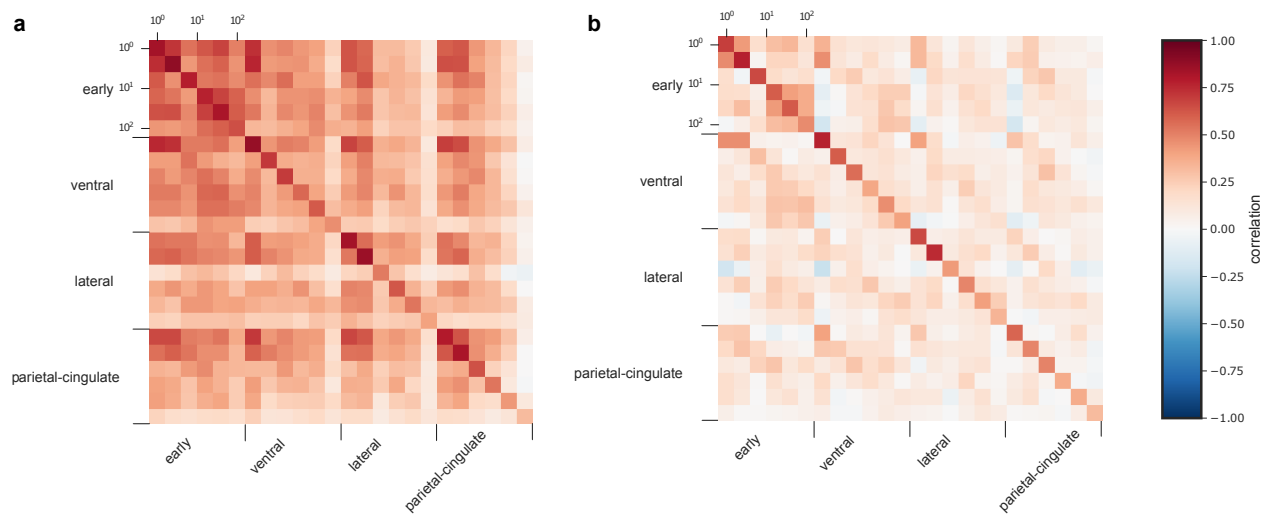


**Figure S3: Region-specific patterns of individual differences emerge at each dimensional range.** (a) Correlation matrices show relationships between individual differences matrices (IDMs) across regions and dimensional ranges. Each element represents the correlation between even-movie IDMs from one range in a region (rows) and odd-movie IDMs from another range in a region (columns). The log-scaled axis labels indicate dimensional ranges. The diagonal blocks show within-region correlations across matching dimensional ranges, while off-diagonal blocks show cross-region correlations. (b) Same analysis after controlling for coarse-scale effects by partialing out voxelwise inter-subject correlations. The more pronounced diagonal structure demonstrates that removing coarse-grained patterns reveals region-specific patterns of individual variability that are unique to each cortical area and dimensional range. This analysis complements Fig. 3 by showing that individual differences not only vary across dimensions within regions but also exhibit distinct patterns across regions at corresponding dimensional ranges.

## References

1. I. Charest, N. Kriegeskorte, The brain of the beholder: honouring individual representational idiosyncrasies. *Language, Cognition and Neuroscience* **30** (4), 367–379 (2015), doi:10.1080/23273798.2014.1002505.
2. E. S. Finn, X. Shen, D. Scheinost, M. D. Rosenberg, J. Huang, M. M. Chun, X. Papademetris, R. T. Constable, Functional connectome fingerprinting: identifying individuals using patterns of brain connectivity. *Nature neuroscience* **18** (11), 1664–1671 (2015).
3. C. Gratton, T. O. Laumann, A. N. Nielsen, D. J. Greene, E. M. Gordon, A. W. Gilmore, S. M. Nelson, R. S. Coalson, A. Z. Snyder, B. L. Schlaggar, *et al.*, Functional brain networks are dominated by stable group and individual factors, not cognitive or daily variation. *Neuron* **98** (2), 439–452 (2018).
4. E. S. Finn, E. Glerean, A. Y. Khojandi, D. Nielson, P. J. Molfese, D. A. Handwerker, P. A. Bandettini, Idiosynchrony: From shared responses to individual differences during naturalistic neuroimaging. *NeuroImage* **215**, 116828 (2020), doi:10.1016/j.neuroimage.2020.116828.
5. E. S. Finn, P. R. Corlett, G. Chen, P. A. Bandettini, R. T. Constable, Trait paranoia shapes inter-subject synchrony in brain activity during an ambiguous social narrative. *Nature Communications* **9** (1), 2043 (2018), doi:10.1038/s41467-018-04387-2.
6. Y. Yeshurun, S. Swanson, E. Simony, J. Chen, C. Lazaridi, C. J. Honey, U. Hasson, Same story, different story: the neural representation of interpretive frameworks. *Psychological science* **28** (3), 307–319 (2017).
7. J. M. Lahnakoski, E. Glerean, I. P. Jääskeläinen, J. Hyönä, R. Hari, M. Sams, L. Nummenmaa, Synchronous brain activity across individuals underlies shared psychological perspectives. *NeuroImage* **100**, 316–324 (2014).
8. S. Fusi, E. K. Miller, M. Rigotti, Why neurons mix: high dimensionality for higher cognition. *Current Opinion in Neurobiology* **37**, 66–74 (2016), neurobiology of cognitive behavior, doi: <https://doi.org/10.1016/j.conb.2016.01.010>, <https://www.sciencedirect.com/science/article/pii/S0959438816000118>.



9. S. R. Lehky, R. Kiani, H. Esteky, K. Tanaka, Dimensionality of Object Representations in Monkey Inferotemporal Cortex. *Neural Computation* **26** (10), 2135–2162 (2014), doi:10.1162/NECO\_a\_00648.
10. J. J. DiCarlo, D. D. Cox, Untangling invariant object recognition. *Trends in cognitive sciences* **11** (8), 333–341 (2007).
11. C. Stringer, M. Pachitariu, N. Steinmetz, M. Carandini, K. D. Harris, High-dimensional geometry of population responses in visual cortex. *Nature* **571** (7765), 361–365 (2019).
12. R. M. Gauthaman, B. Ménard, M. F. Bonner, Universal scale-free representations in human visual cortex (2024), <https://arxiv.org/abs/2409.06843>.
13. J. M. Shine, M. Breakspear, P. T. Bell, K. A. Ehgoetz Martens, R. Shine, O. Koyejo, O. Sporns, R. A. Poldrack, Human cognition involves the dynamic integration of neural activity and neuromodulatory systems. *Nature neuroscience* **22** (2), 289–296 (2019).
14. J. Misra, S. G. Surampudi, M. Venkatesh, C. Limbachia, J. Jaja, L. Pessoa, Learning brain dynamics for decoding and predicting individual differences. *PLoS Computational Biology* **17** (9), e1008943 (2021).
15. C. Lee, J. Han, M. Feilong, G. Jiahui, J. Haxby, C. Baldassano, Hyper-HMM: aligning human brains and semantic features in a common latent event space. *Advances in Neural Information Processing Systems* **36**, 27005–27019 (2023).
16. J. V. Haxby, J. S. Guntupalli, A. C. Connolly, Y. O. Halchenko, B. R. Conroy, M. I. Gobbini, M. Hanke, P. J. Ramadge, A common, high-dimensional model of the representational space in human ventral temporal cortex. *Neuron* **72** (2), 404–416 (2011).
17. C. Sava-Segal, C. Richards, M. Leung, E. S. Finn, Individual differences in neural event segmentation of continuous experiences. *Cerebral Cortex* **33** (13), 8164–8178 (2023), doi: 10.1093/cercor/bhad106, <https://doi.org/10.1093/cercor/bhad106>.
18. M. Feilong, S. A. Nastase, J. S. Guntupalli, J. V. Haxby, Reliable individual differences in fine-grained cortical functional architecture. *NeuroImage* **183**, 375–386 (2018).

19. C. Spearman, The proof and measurement of association between two things. (1961).
20. A. Krizhevsky, I. Sutskever, G. E. Hinton, ImageNet classification with deep convolutional neural networks. *Communications of the ACM* **60** (6), 84–90 (2017).
21. K. He, X. Zhang, S. Ren, J. Sun, Deep residual learning for image recognition, in *Proceedings of the IEEE conference on computer vision and pattern recognition* (2016), pp. 770–778.
22. A. Dosovitskiy, L. Beyer, A. Kolesnikov, D. Weissenborn, X. Zhai, T. Unterthiner, M. Dehghani, M. Minderer, G. Heigold, S. Gelly, *et al.*, An image is worth 16x16 words: Transformers for image recognition at scale. *arXiv preprint arXiv:2010.11929* (2020).
23. A. Vaswani, N. Shazeer, N. Parmar, J. Uszkoreit, L. Jones, A. N. Gomez, L. Kaiser, I. Polosukhin, Attention is all you need. *Advances in neural information processing systems* **30** (2017).
24. T. Brown, B. Mann, N. Ryder, M. Subbiah, J. D. Kaplan, P. Dhariwal, A. Neelakantan, P. Shyam, G. Sastry, A. Askell, *et al.*, Language models are few-shot learners. *Advances in neural information processing systems* **33**, 1877–1901 (2020).
25. J. Kaplan, S. McCandlish, T. Henighan, T. B. Brown, B. Chess, R. Child, S. Gray, A. Radford, J. Wu, D. Amodei, Scaling laws for neural language models. *arXiv preprint arXiv:2001.08361* (2020).
26. E. J. Allen, G. St-Yves, Y. Wu, J. L. Breedlove, J. S. Prince, L. T. Dowdle, M. Nau, B. Caron, F. Pestilli, I. Charest, *et al.*, A massive 7T fMRI dataset to bridge cognitive neuroscience and artificial intelligence. *Nature neuroscience* **25** (1), 116–126 (2022).
27. M. N. Hebart, O. Contier, L. Teichmann, A. H. Rockter, C. Y. Zheng, A. Kidder, A. Corriveau, M. Vaziri-Pashkam, C. I. Baker, THINGS-data, a multimodal collection of large-scale datasets for investigating object representations in human brain and behavior. *Elife* **12**, e82580 (2023).
28. J. Manley, S. Lu, K. Barber, J. Demas, H. Kim, D. Meyer, F. M. Traub, A. Vaziri, Simultaneous, cortex-wide dynamics of up to 1 million neurons reveal unbounded scaling of dimensionality with neuron number. *Neuron* **112** (10), 1694–1709 (2024).

29. O. Contier, C. I. Baker, M. N. Hebart, Distributed representations of behaviour-derived object dimensions in the human visual system. *Nature Human Behaviour* **8** (11), 2179–2193 (2024).
30. E. Elmoznino, M. F. Bonner, High-performing neural network models of visual cortex benefit from high latent dimensionality. *PLoS computational biology* **20** (1), e1011792 (2024).
31. B. Sorscher, S. Ganguli, H. Sompolinsky, Neural representational geometry underlies few-shot concept learning. *Proceedings of the National Academy of Sciences* **119** (43), e2200800119 (2022).
32. J. S. Guntupalli, *Hyperaligning Neural Representational Spaces* (Springer US, New York, NY), p. 281–289 (2020), doi:10.1007/7657\_2019\_25, [https://doi.org/10.1007/7657\\_2019\\_25](https://doi.org/10.1007/7657_2019_25).
33. M. Feilong, J. S. Guntupalli, J. V. Haxby, The neural basis of intelligence in fine-grained cortical topographies. *eLife* **10**, e64058 (2021), doi:10.7554/eLife.64058.
34. L. Posani, S. Wang, S. P. Muscinelli, L. Paninski, S. Fusi, Rarely categorical, always high-dimensional: how the neural code changes along the cortical hierarchy. *bioRxiv* pp. 2024–11 (2025).
35. U. Hasson, G. Avidan, H. Gelbard, I. Vallines, M. Harel, N. Minshew, M. Behrmann, Shared and idiosyncratic cortical activation patterns in autism revealed under continuous real-life viewing conditions. *Autism Research* **2** (4), 220–231 (2009).
36. E. S. Finn, R. Todd Constable, Individual variation in functional brain connectivity: implications for personalized approaches to psychiatric disease. *Dialogues in clinical neuroscience* **18** (3), 277–287 (2016).
37. T. A. Bolton, D. Jochaut, A.-L. Giraud, D. Van De Ville, Brain dynamics in ASD during movie-watching show idiosyncratic functional integration and segregation. *Human brain mapping* **39** (6), 2391–2404 (2018).
38. J. Salmi, M. Metwaly, J. Tohka, K. Alho, S. Leppämäki, P. Tani, A. Koski, T. Vanderwal, M. Laine, ADHD desynchronizes brain activity during watching a distracted multi-talker conversation. *NeuroImage* **216**, 116352 (2020).

39. Z. Yang, J. Wu, L. Xu, Z. Deng, Y. Tang, J. Gao, Y. Hu, Y. Zhang, S. Qin, C. Li, *et al.*, Individualized psychiatric imaging based on inter-subject neural synchronization in movie watching. *NeuroImage* **216**, 116227 (2020).
40. O. Esteban, C. J. Markiewicz, R. W. Blair, C. A. Moodie, A. I. Isik, A. Erramuzpe, J. D. Kent, M. Goncalves, E. DuPre, M. Snyder, H. Oya, S. S. Ghosh, J. Wright, J. Durnez, R. A. Poldrack, K. J. Gorgolewski, fMRIPrep: a robust preprocessing pipeline for functional MRI. *Nature Methods* **16** (1), 111–116 (2019), doi:10.1038/s41592-018-0235-4, <https://doi.org/10.1038/s41592-018-0235-4>.
41. S. M. Smith, M. Jenkinson, M. W. Woolrich, C. F. Beckmann, T. E. Behrens, H. Johansen-Berg, P. R. Bannister, M. De Luca, I. Drobnjak, D. E. Flitney, *et al.*, Advances in functional and structural MR image analysis and implementation as FSL. *Neuroimage* **23**, S208–S219 (2004).
42. E. T. Rolls, C.-C. Huang, C.-P. Lin, J. Feng, M. Joliot, Automated anatomical labelling atlas 3. *NeuroImage* **206**, 116189 (2020), doi:<https://doi.org/10.1016/j.neuroimage.2019.116189>, <https://www.sciencedirect.com/science/article/pii/S1053811919307803>.
43. N. Kriegeskorte, M. Mur, P. A. Bandettini, Representational similarity analysis-connecting the branches of systems neuroscience. *Frontiers in systems neuroscience* **2**, 249 (2008).
44. D. Cer, Y. Yang, S.-y. Kong, N. Hua, N. Limtiaco, R. S. John, N. Constant, M. Guajardo-Cespedes, S. Yuan, C. Tar, *et al.*, Universal sentence encoder. *arXiv preprint arXiv:1803.11175* (2018).